Article

A Theoretical and Test Analysis of Heat and Humidity Transfer for Deeply Buried Underground Corridors with Different Shapes

Tong Ren *, Mengzhuo Li [ID], Long He [ID], De Wang and Lingbo Kong *

College of Mechanical and Electrical Engineering, Shaanxi University of Science and Technology,
Xi'an 710021, China; 240512146@sust.edu.cn (D.W.)
* Correspondence: rentong@sust.edu.cn (T.R.); lbkong@sust.edu.cn (L.K.)

Abstract: Moisture generation in the ventilation projects of deeply buried underground corridors affects the underground building environment and personnel health. In order to master the heat and humidity transfer law of underground corridors, this paper establishes a mathematical model by theoretical analysis, and the application of the theoretical model in engineering calculation is verified by a field test. It is found that the ventilation efficiency and heat and humidity transfer effect are related to corridor shape. The results show that under the same cross-sectional area, the average temperature drop and humidity of a rectangular corridor are 0.25% and 0.3% higher than that of an arch corridor, and 0.8% and 0.9% higher than that of a circular corridor. Under the condition of constant section circumference, the average temperature drop and humidity of a rectangular corridor are 0.51% and 0.62% higher than that of an arch corridor, and 1.37% and 1.58% higher than that of a circular corridor. When the equivalent diameter is the same, there is almost no difference in the heat and humidity transfer effect of the three shaped corridors.

Keywords: underground corridor; corridor shape; heat and humidity transfer; field test; mathematical model

1. Introduction

As the world's leading energy consumer, China is facing substantial energy and environmental issues due to rapid industrialization and urbanization. The government prioritizes renewable energy development and has established comprehensive laws and policies to foster its growth [1]. At present, many studies are trying to save energy and reduce emissions. There are several ways to change the situation of air pollution and energy shortage, such as improving efficiency, developing biofuels, and researching clean energy [2]. China's hydropower generation holds a significant position on the global stage. In 2020, it accounted for 30.8% of the world's total hydropower output, securing the top rank internationally. Furthermore, China's installed hydropower capacity, including pumped storage, reached 370,160 MW, representing 27.8% of the global total and also ranking first worldwide [3,4]. As hydropower stations are built underground, there are many corridors in the underground hydropower station, and the traffic tunnel is one of the most important corridors. It not only assumes transportation but also shoulders the responsibility of underground environmental ventilation to provide fresh air [5]. In the ventilation system of an underground power station powerhouse, the energy storage capacity of the underground corridor in a hydropower station is often used to pre-cool or pre-heat the ventilation air, which has become an effective, renewable, economical, and practical ventilation mode, and this ventilation mode has been widely used in the design of the ventilation system of the hydropower station [6–8]. In the actual project, there are a

large number of other underground buildings, such as subways, integrated pipe corridors, mines, and so on, and it has been found that this type of processing is also applicable to them.

The underground space of a hydropower station consists of many tunnels, conjunction nodes, connected corridors, and large plants, which form a cavern group [9]. An underground traffic tunnel is a large and long pipe buried deep underground. According to its narrow and long characteristics, the temperature distribution of one-dimensional flow along with naturally ventilated tunnels can be obtained based on studies with theoretical simplification [10]. In order to conduct research on ventilation and heat transfer in underground corridors, a large number of researchers have contributed in this regard. In Refs. [11,12], the authors studied the wall heat transfer coefficient and the law of the change in airflow temperature in underground caverns and obtained the formula of dynamic ventilation temperature calculation and the determination method of the wall heat transfer coefficient. In Ref. [13], the authors used Green's function method to solve the problem of heat transfer in underground space. Ref. [14] verified the cooling and dehumidification effects of underground tunnels on air by comparing numerical simulation with empirical formulas. Based on the study of air temperature distribution characteristics in corridors, Ref. [15] calculated the variation of the heat transfer coefficient with wall temperature, heat dissipation, and cross-section wind speed by CFD (Computational Fluid Dynamics) simulation and discussed the limit length for the ventilation corridor. Another study, in order to understand and predict the temperature field in and around a surrounding rock tunnel, successfully derived the governing equations of heat conduction in the surrounding rock and air flow and heat flow transfer in the tunnel, respectively, taking into account the conservation of mass, momentum, and energy [16,17].

In the process of ventilation through the corridor, the underground power station brings a lot of "moisture" to the corridor and indoors, leading to condensation and fog in the corridor and resulting in a humid environment in the factory building, which makes the staff perspire, creating an environment for microorganisms and bacteria to breed, as shown in Figure 1. Therefore, in the study of heat transfer in underground corridors, some studies have considered moisture transfer between corridors and air. In Refs. [18,19], the authors established the differential equation of the moisture transfer process according to the physical model of moisture transfer in the underground tunnel wall and obtained the theoretical calculation formula for moisture dissipation on the wall. Ref. [20] introduced an analytical model utilizing the superposition method to calculate condensation along the flow path. Subsequently, a numerical calculation method was developed, enabling rapid and dynamic computation of heat and humidity exchange between air and the corridor [21]. However, this model incorporated a wall moisture transfer coefficient, which posed a challenge in practical calculations due to its difficulty in determining. Another study [22] proposed the thermal and humid environment control scheme of underground protection engineering by using the DEA (Data Envelopment Analysis) evaluation method and gave practical examples to provide methods for the control of the wet environment of underground engineering. Another study [23] developed a numerical model to investigate the impact of airflow on the temperature distribution within the surrounding rock of a tunnel. They concluded that airflow temperature and velocity are the two most critical factors influencing the temperature field of the surrounding rock.

In the above review, the authors found that the common assumption of theoretical simplification research is that the underground corridor is simplified to a cylindrical shape, and the heat and humidity in the corridor are considered the heat conduction and mass transfer of air through the cylinder. However, in the construction of hydroelectric power stations, the authors found that there are many types of underground corridor structures,

such as circular tunnels, rectangular tunnels, and arch tunnels, as shown in Figure 2. In Ref. [24], the author conducted an in-depth analysis of the impact of pipe geometry, length, diameter, and other parameters on the heat transfer efficiency of soil heat exchange systems through numerical simulations. This indicates that designing more intricate pipe configurations can substantially enhance the system's heat transfer performance. At the same time, a gas migration model within the tunnel through computational fluid dynamics numerical simulation was studied. It provided an in-depth discussion on the impact of various parameters, including pipe diameters and the distance between the pipe entrance and the working face, on both the tunnel airflow field and gas distribution patterns. The findings indicate that the diameter of the air duct significantly influences the gas volume fraction field at the working face [25]. In order to study the differences between advanced tunnels and typical tunnels in a smoky environment, an empirical model for temperature prediction was compared by experiments and simulations. The results show that the model effectively describes the longitudinal temperature attenuation process of fire smoke in a propulsion tunnel, considering different section shapes [26]. In addition, a numerical investigation into the longitudinal positioning of fire sources within inclined tunnels under natural ventilation conditions was researched, and it indicates that in longitudinally inclined tunnels, the height of the neutral plane is primarily influenced by both the longitudinal position and slope of the fire source while exhibiting relative insensitivity to variations in heat release rate [27]. Another study designed four terra-tunnel reference cases: three fire sources at different locations and one with smoke ventilation turned off. The analysis takes into account temperature distribution and gas flow rates, as well as qualitatively validates visibility. The results showed that the variant in which the fire source was located in the middle of the corridor proved to be the most disadvantageous variant in terms of the effectiveness of smoke ventilation [28].

| (a) | (b) | (c) |
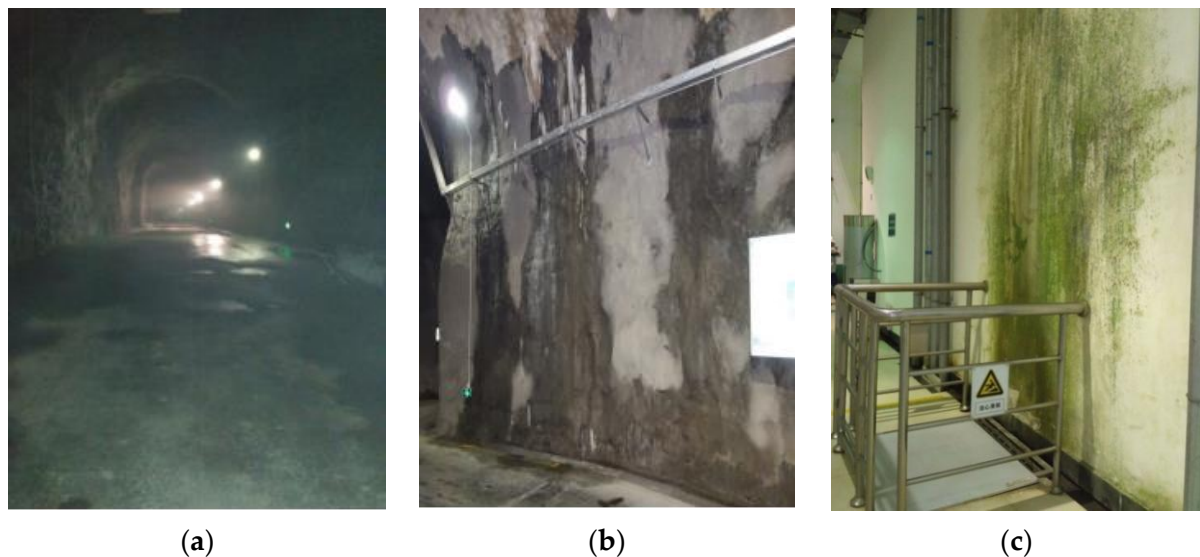
Figure 1. Wet environment of underground corridor and plant. (**a**) Fog in the corridor. (**b**) Damp gallery walls. (**c**) Mildew on the factory walls.

The methods to solve the heat and humidity transfer model include numerical simulation, theoretical analysis, and experimental testing [29]. When the mathematical model is too complex and the numerical calculation is too heavy to implement, the numerical simulation is the most effective and reliable method [30]. Experimental testing can obtain the data in the actual operating environment, which has high reliability, but the data collection process is time-consuming [31]. The theoretical analysis can predict the temperature and humidity of the air flow in the tunnel and provide a reliable theoretical basis for the

control of the thermal environment in the process of tunnel ventilation. However, the actual situation may be too simplified to cover all the actual influencing factors [32]. In this paper, a combination of theoretical analysis and field test can simulate the moisture and heat distribution of tunnel air flow accurately and comprehensively.

Figure 2. Types of corridors in actual engineering. (**a**) Rectangular tunnel. (**b**) Circular tunnel. (**c**) Arch tunnel.

In this paper, the physical model of the underground power station corridor and its internal thermal and humid environment are described and analyzed. A mathematical equation of heat and humidity transfer of underground corridors is established and the relationship between convective heat and moisture transfer between the underground corridor and the air is obtained. Based on this, the heat and humidity transfer prediction formulas for circular corridors, arch corridors, and rectangular corridors are proposed. The air temperature, relative humidity, wall temperature, and other parameters in the corridors of three power stations were collected to verify the rationality and accuracy of the theoretical calculation formula. At the same time, based on the comparative analysis of the measured field data and the calculation formula, the influence of the geometric parameters of the corridor (cross-section area, equivalent diameter, cross-section circumference) on heat and humidity transfer is analyzed.

2. Corridor Mathematical Model

2.1. Environmental Influencing Factors and Assumptions of Underground Tunnels

In the process of analyzing the heat and moisture exchange between the underground corridor and the flowing air, it is difficult to establish an equation for the heat and moisture balance of the air in the corridor completely according to the actual situation. There are many factors that influence the thermophysical properties of a corridor, such as groundwater level, moisture source, etc. [10,32–37]. So, the following assumptions are made [4]:

(1)　The air in the corridor is treated as an incompressible fluid.
(2)　The rock stratum in the underground corridor is an isotropic and homogeneous medium, and the physical parameters of the rock stratum are constant.
(3)　Because the length of the corridor is much larger than the cross-sectional size of the corridor, only the changes in heat and humidity among the length direction are considered.
(4)　Ignore fluctuation of ground temperature and the influence of radiation [36].

2.2. Mathematical Model of Heat and Moisture Transfer in the Corridor

Combined with the rotating curved surface in mathematics [38], it can be regarded as an irregular corridor in the underground power station. The variation law of air tempera-

ture and humidity in the corridor is studied. The mathematical model of air temperature, humidity, and enthalpy distribution in the heat and humidity exchange process of the rotating curved surface corridor is established by the infinitesimal integral method, and a basic heat and humidity calculation equation of corridor ventilation is derived.

Assuming that in a continuous ventilation system, after an infinite period of sufficient cooling, the heat and moisture exchange between the air and the corridor tends to be balanced, the corridor is divided into several unit sections along the *x*-axis direction, and each tiny unit can be regarded as a stable heat and moisture transfer area. Figure 3 is a schematic diagram of heat and moisture transfer in a rotating curved corridor, taking a small distance d*x* along the rotating axis and establishing a heat balance equation there. Suppose the air flow is *G* and flows in the *x* direction, as shown by the arrow in Figure 3.
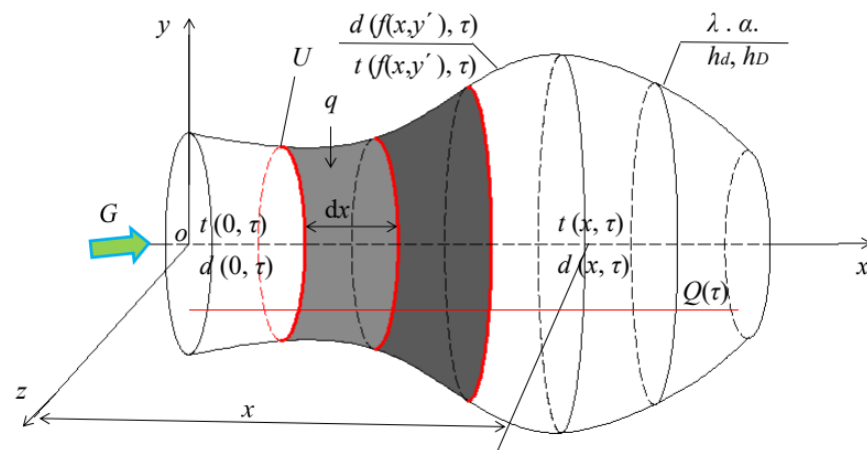

Figure 3. Schematic diagram of the corridor with a rotary surface.

$$cG\left[\frac{\partial t(x,\ \tau)}{\partial x}dx\right] = \alpha U\left[t(f(x,\ y'),\ \tau) - t(x,\ \tau)\right]dx + Qdx \tag{1}$$

$$-\lambda \left|\frac{\partial t(f(x,\ y'),\ \tau)}{\partial f(x,\ y')}\right|_{f(x,\ y')=f} = \alpha\left[t(x,\ \tau) - t(f(x,\ y'),\ \tau)\right] - Q \tag{2}$$

Initial condition $\tau = 0, t(f(x,y'),\tau) = t_T$. Boundary condition $x = 0, t(f(0,y'),\tau) = t_0$. The symbols in the formula and the figure, respectively, indicate:

$t(x,\ \tau)$⁻τ Air temperature at the depth x m of the corridor at all times, °C; $t(f(x,\ y'),\ \tau)$⁻τ Temperature of the rock wall of the corridor time, °C; t_0—Air temperature at the entrance of the corridor, °C; $f(x,\ y')$—Equivalent radius of the rotating surface corridor, m; U—Wet circumference of the cross-section of the rotating curved corridor, m; x—Distance within the corridor from the entrance of the corridor, m; G—Air flow, kg/s; Q—Heat source intensity, W/m; τ—Time, s; λ—Wall thermal conductivity, W/(m · °C); α—Surface heat transfer coefficient [38], W/(m²·°C).

$$\alpha = 2.25\left[0.02\frac{\lambda}{d}\text{Re}^{0.8}\right] \tag{3}$$

where, Re—Reynolds criterion; Re $=\frac{vC}{\lambda}$ *C*—Equivalent diameter of underground corridor, m.

$$C = \frac{4F}{U} \text{ m.}$$

According to the initial conditions and boundary conditions, the differential equation can be solved, and the mathematical analytical formula of the air temperature distribution in the corridor with the infinite rotating surface can be calculated, namely:

$$t_{x,\tau} = t_0 + \left(\frac{Q}{qU} - t_0 + t_T \right) \left(1 - e^{-\frac{qUx}{cG}} \right) \tag{4}$$

When $Q = 0$, the above formula is

$$t_{x,\tau} = t_T + (t_0 - t_T) e^{-\frac{qUx}{cG}} \tag{5}$$

By the same token, the equilibrium equation of moisture exchange in a rotating curved surface corridor is as follows:

$$G \frac{d(d(x,\tau))}{d_x} d_x = h_D U \left[d_{f(x,y')}(x,\tau) - d(x,\tau) \right] d_x \tag{6}$$

Initial condition $\tau = 0, t(f(x,y'),\tau) = d_D$.
Boundary condition $x = 0, t(f(0,y'),\tau) = d_0$.
The symbols in the formula and the figure, respectively, indicate: $d(x,\tau)$—τ moisture content of air at the depth x m section of the corridor at time, g/kg; $d(f(x,y'),\tau)$—τ Moisture content in corridor wall at all times, g/kg; d_0—Moisture content of air at the entrance of corridor, g/kg; d_D—Moisture content of rock mass wall, g/kg; h_D—Mass diffusion flux per unit surface area per unit time; $h_D = \frac{h_d}{\rho}$; ρ—Air density, kg/m^3; h_d—Mass transfer coefficient driven by air moisture difference, kg/(m^2·s).

$$\text{Air dehumidification process}: h_d = \frac{\rho}{3600}(11.3v + 12.1) \tag{7}$$

$$\text{Air humidification process}: h_d = \frac{\rho_a}{3600}(16.2v + 22.3) \tag{8}$$

According to the initial conditions and boundary conditions, the differential equation can be solved, and the mathematical analytical formula of air humidity distribution in a rotating curved corridor can be calculated as follows:

$$\text{Namely } d_{x,\tau} = d_D + (d_0 - d_D) e^{-\frac{h_D U x}{G}} \tag{9}$$

Calculated by the moisture content of humid air:

$$d_{x,\tau} = 0.622 \frac{\varphi(x,\tau) p_{q,b}(x,\tau)}{B - \varphi(x,\tau) p_{q,b}(x,\tau)} \tag{10}$$

Taking in (8), the mathematical analytical formula of air relative humidity distribution of air along the rotating curved surface corridor can be obtained:

$$\varphi(x,\tau) = \frac{B}{p_{q,b}(x,\tau)} \cdot \frac{d_D + (d_0 - d_D) e^{-\frac{h_D U x}{G}}}{0.622 + d_D + (d_0 - d_D) e^{-\frac{h_D U x}{G}}} \times 100\% \tag{11}$$

In the formula: $\varphi(x,\tau)$—The relative humidity of the air at the depth x m of the corridor at time τ, %; B—Local atmospheric pressure, Pa; $P_{q,b}(x,\tau)$—The partial pressure of saturated water vapor in the air at x m depth in the corridor at time τ, Pa.

$$\text{Among them, } p_{q,b}(x,\tau) = exp\left(\frac{c_1}{T} + c_2 + c_3 T + c_4 T^2 + + c_5 T^3 + c_6 T^4 + c_7 lnT \right)$$

$$T = t(x,\tau) + 273.15 \tag{12}$$

$c_1 = -5800.2206$, $c_2 = 1.3914993$, $c_3 = -0.04860239$, $c_4 = 0.41764768 \times 10^{-4}$, $c_5 = -0.14452093 \times 10^{-7}$, $c_6 = 0$, $c_7 = 6.5459673$

The simplified mathematical analytical formula of the air enthalpy distribution in the rotating surface corridor can be obtained by bringing the calculation formulas of the air temperature and humidity distribution (5) and (10) into the enthalpy calculation of the following Formula (13), respectively:

$$h(x,\ \tau) = 1.01t(x,\ \tau) + (2500 + 1.84t(x,\ \tau))d(x,\ \tau) \tag{13}$$

Bring into the above formula: $t(x,\ \tau), d(x,\ \tau)$

$$h(x,\tau) = 1.01t_T + 1.01(t_0 - t_T)e^{-\frac{qUx}{cG}} + \left[2500 + 1.84t_T + 1.84(t_0 - t_T)e^{-\frac{qUx}{cG}} \right] \cdot \left[d_D + (d_0 - d_D)e^{-\frac{h_DUx}{G}} \right] \tag{14}$$

Therefore, according to the above push-down formula, when the envelope of the size of an underground corridor $(U,\ x)$, air temperature $(t_{i,\ \tau})$, relative humidity $(\phi_{i,\ \tau})$, flow rate, wall temperature (t_w), humidity (ϕ_w), and other conditions is known, the distribution of air temperature, humidity, relative humidity, and enthalpy along the length of the underground corridor at different times under outdoor air parameters can be calculated.

3. Mathematical Model of Heat and Moisture Transfer in an Arched Corridor

Figure 4 is a schematic diagram of an arched corridor. The air flows in the x direction and exchanges heat with the tunnel wall. In order to obtain the temperature and humidity distribution of the air in the tunnel, the fractional method is used in this paper. Other heat sources in the tunnel are simplified to the line heat source $Q_{(\tau)}$ for processing. In the axial direction of the arched tunnel, a small distance dx is taken and the equation of heat balance is established in this place, that is, the heat dissipation per unit length of air flowing through the corridor is equal to the heat exchange between air and rock in the corridor per unit length. Then, the integral of the element dx can establish the temperature and humidity distribution of the air in the tunnel.
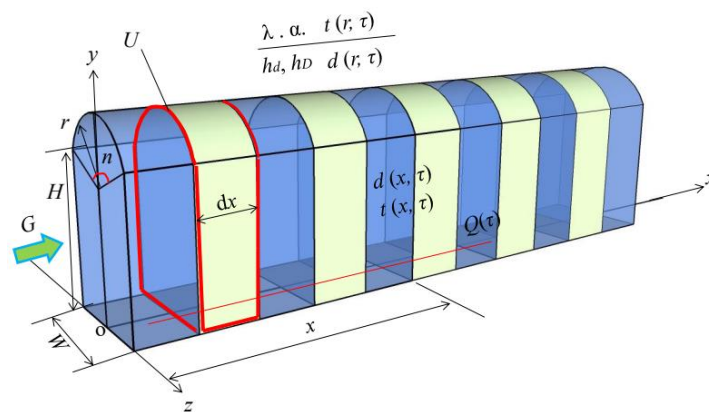

Figure 4. Schematic of the arch corridor.

According to the initial conditions and boundary conditions, the differential equation can be solved, and the mathematical analytical formula of the air temperature distribution in an infinite arched corridor can be calculated:

$$t_{x,\ \tau} = t_T + \left(\frac{Q}{q\left(2H + W + \frac{n\pi r_0}{180}\right)} - t_0 + t_T \right) \left(1 - e^{-\frac{q\left(2H + W + \frac{n\pi r_0}{180}\right)x}{cG}} \right) \tag{15}$$

Among them, the cross-sectional perimeter of the arch is

$$U = 2H + W + \frac{n\pi r_0}{180} \tag{16}$$

When $Q = 0$,
the above Equation (15) can be simplified to

$$t_{x,\tau} = t_T + (t_0 - t_T)e^{-\frac{q(2H+W+\frac{n\pi r_0}{180})x}{cG}} \tag{17}$$

where

U—Wet circumference of the cross-section of the corridor, m, for the arched corridor, $U = 2H + W + \frac{n\pi r_0}{180}$;

H—Height of arched corridor, m;

W—Width of arched corridor, m;

n—The angle of the vault arch of the arched corridor, (°);

r_0—Radius of arch corridor vault arc, m.

By integrating the mathematical differential equation of moisture transfer, the mathematical analytical formula of the moisture distribution of the arch can be obtained:

$$d_{x,\tau} = d_D + (d_0 - d_D)e^{-\frac{h_D(2H+W+\frac{n\pi r}{180})x}{G}} \tag{18}$$

Consequently, the mathematical analytical formula for the relative humidity distribution of the air in the arched corridor is obtained:

$$\varphi(x,\tau) = \frac{B}{p_{q,b}(x,\tau)} \cdot \frac{d_D + (d_0 - d_D)e^{-\frac{h_D(2H+W+\frac{n\pi r_0}{180})x}{G}}}{0.622 + d_D + (d_0 - d_D)e^{-\frac{h_D(2H+W+\frac{n\pi r_0}{180})x}{G}}} \times 100\% \tag{19}$$

Accordingly, the mathematical analytical formula for the air enthalpy distribution in the arched corridor is obtained:

$$h(x,\tau) = 1.01t_T + 1.01(t_0 - t_T)e^{-\frac{q(2H+W+\frac{n\pi r_0}{180})x}{cG}} + \left[2500 + 1.84t_T + 1.84(t_0 - t_T)e^{-\frac{q(2H+W+\frac{n\pi r_0}{180})x}{cG}}\right]$$
$$\cdot \left[d_D + (d_0 - d_D)e^{-\frac{h_D(2H+W+\frac{n\pi r_0}{180})x}{G}}\right] \tag{20}$$

4. Field Measurement and Results

4.1. Field Tests

In this paper, the heat absorption and release effects of rock walls and the air temperature and humidity distribution law were tested along the length of underground corridors of hydroelectric power stations in three regions of China. Figure 5 shows the regional distribution and information of the field test hydropower station.
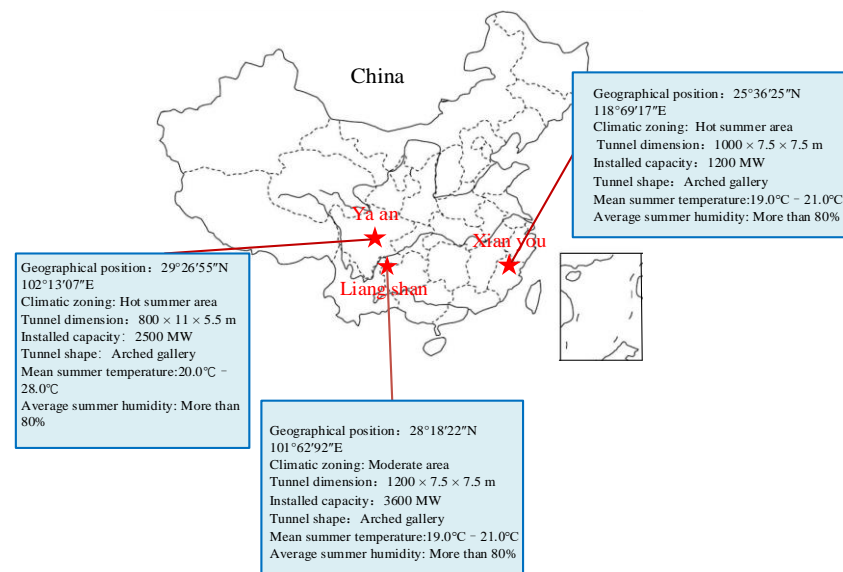
Figure 5. Regional distribution of the field test hydropower station.

4.2. Test Contents and Instruments

The field test mainly includes the following parameters, and the main instruments used are shown in Table 1:

(1) Air parameters inside and outside the corridor: air dry bulb temperature, relative humidity, and wind speed. Select TSI anemometer (temperature, humidity, and wind speed are recorded at the same time) for testing;

(2) Air parameters and rock wall temperature at different positions in the traffic tunnel: air dry bulb temperature, relative humidity, rock wall temperature. Among them, the air temperature and humidity parameters in the traffic tunnel are continuously measured for 24 h. The test instrument is RR002, the self-recorder of temperature and humidity of the China Architecture Research Institute, and the data recording interval is selected as 30 min;

(3) According to the actual situation of the traffic tunnel structure on site, the measurement points of the temperature and humidity modules are arranged at equal intervals. The tool used is the infrared rangefinder (measuring range 300 m); the temperature and humidity self-recorder is hung 2 m from the ground at these measuring points and the outdoor temperature and relative humidity are hung in the place without direct sunlight for 24 h uninterrupted measurement;

(4) For the wind speed at different positions in the traffic tunnel, the average wind speed of the section is measured by the TSI wind speed tester at the measuring points of the characteristic section in the traffic tunnel, and the average wind speed is the average value of each measurement point of the section; the temperature of the wall was measured using an infrared laser thermometer.

**Table 1.** List of main testing instruments.

| Serial Number	Schematic Diagram of Instrument	Name of Instrument	Instrument Model	Manufacturer	Accuracy and Measurement Range
1		Single-channel portable hotline Velocimeter	8386A	TSI (Shoreview, MN, USA)	Temperature, ± 0.3 °C, (-17.89 to 3.3 °C) Wind speed, $\pm 3\%$, (0–50 m/s) Relative humidity, $\pm 3\%$ RH, (0–95% RH)

Serial Number	Schematic Diagram of Instrument	Name of Instrument	Instrument Model	Manufacturer	Accuracy and Measurement Range
2		Temperature and humidity recorder	RR002	Zhongyi Environmental Science Technology Co., LTD (Suzhou, China)	Temperature, $\pm 3\,^{\circ}C$, (-10 to $50\,^{\circ}C$)
3		Infrared thermometer (Wall temperature test)	FLUKE-66	FLUKE (Everett, WA, USA)	Temperature, $\pm 3\,^{\circ}C$ (-32 to $-26\,^{\circ}C$), $\pm 2.5\,^{\circ}C$, (-26 to -1), $8 \pm 2\,^{\circ}C$, (-18 to $23\,^{\circ}C$)
4		Infrared rangefinder	Leica-S910	Leica (Teaneck, NJ, USA)	Distance, ± 1.0 mm, (0.05–300 m)

4.3. Layout of Measuring Points and Processing Method of Testing Data

Taking the arched corridor as an example, when arranging the measuring points of the underground arched corridor, firstly, the cross-section of the corridor is divided geometrically, and the measuring points are arranged at the geometric center. In the horizontal direction of the corridor, the measuring points are arranged at a height of 2 m along the central axis, as shown in Figure 6, and Figure 7 is the measured field photos of Jinping Power Station.

(a)

(b)
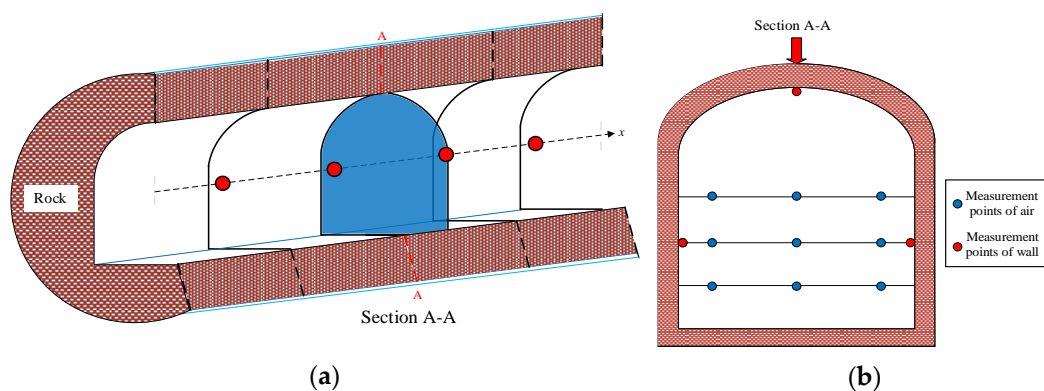
Figure 6. Dependent layout diagram of the floor corridor measuring points. (**a**) Arrangement of measuring points in the length direction. (**b**) Arrangement of measuring points in cross-section.

(a)

(b)

(c)
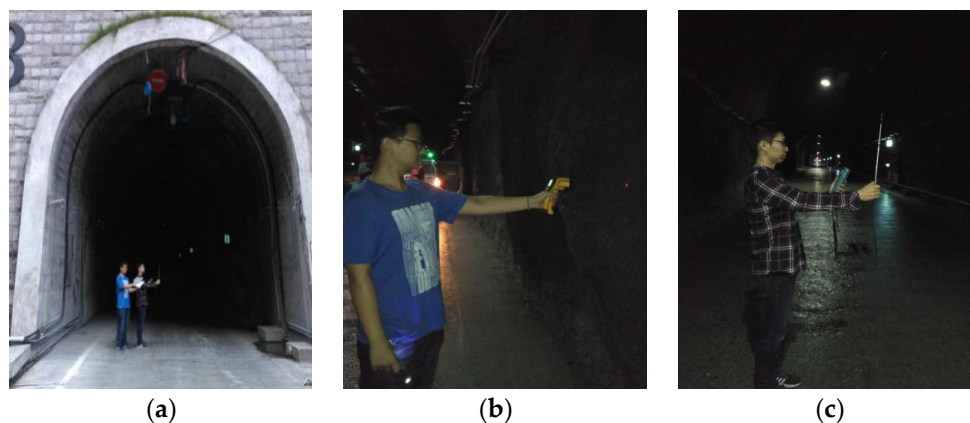
Figure 7. Field test of the underground corridor. (**a**) Inlet air parameter test. (**b**) Corridor wall temperature test. (**c**) Wind speed test in corridor.

In this paper, we treat the temperature, velocity, moisture content, distance, and enthalpy as dimensionless for comparison.

In this study, in order to evenly compare the temperature changes under different working conditions, dimensionless temperature is adopted, which is determined by the following formula:

$$\theta = \frac{t_i - t_T}{t_0 - t_T} \tag{21}$$

where θ is the dimensionless temperature, t_i is the temperature at measuring point, t_0 is the inlet air temperature, and t_T is the wall temperature.

The formula for dimensionless moisture content is as follows:

$$w = \frac{d_i}{d_0} \tag{22}$$

where w is dimensionless moisture content and d_i is the moisture content a of each measuring point, g/kg. d_0 is the moisture content of inlet, g/kg.

The formula for dimensionless distance is as follows:

$$l = \frac{L_i}{L} \tag{23}$$

where l is dimensionless distance and L_i is the distance of the measuring point from the entrance, m. L is the tunnel length m.

The formula for dimensionless enthalpy is as follows:

$$h_0 = \frac{H_i}{H_0} \tag{24}$$

where h_0 is dimensionless enthalpy and H_i is the enthalpy of the measuring point, kJ/kg. H_0 is the enthalpy of the inlet, kJ/kg.

*4.4. Test Results of Each Power Station*

Combined with the actual situation of the incoming traffic tunnel of the Xianyou Power Station, measuring points were arranged at 10 m, 600 m, and 1000 m away from the entrance of the incoming traffic tunnel. The air and heat transfer characteristics of the underground traffic corridor of the Xianyou Power Station were continuously tested for 96 h.

From the analysis of Figure 8a, it can be seen that the temperature and temperature rise curve of the traffic tunnel is close to the logarithmic curve, with a large slope at the beginning and then gradually decreasing, and the maximum temperature difference between the entrance and the end of traffic tunnel is 5.8 °C. Therefore, the section from the entrance of the traffic tunnel plays a major role in regulating the air supply temperature, and the farther away from the entrance, the weaker the regulating ability. The type of relative humidity curve is the same as that of the temperature curve but the difference is that the trend is just the opposite. The relative humidity of the measuring point at 510 m is as high as 100%. In the field test, it was found that the fog phenomenon can be observed obviously in the traffic tunnel at a distance of 500~800 m from the entrance, and there was condensed water on the surface of the tunnel wall. At the same time, it can be seen that the wall temperature changes at different positions and there is a sudden drop at the beginning, which is due to the great influence of outdoor factors on the entrance. Then, it gradually descends because the traffic tunnel shows a downward trend; at the deepest buried depth, the maximum temperature difference between the entrance and the end is 5.1 °C, and the overall temperature drop is obvious. The sudden rise in the wall temperature at some measuring points is due to the local installation of strong light sources for illumination in
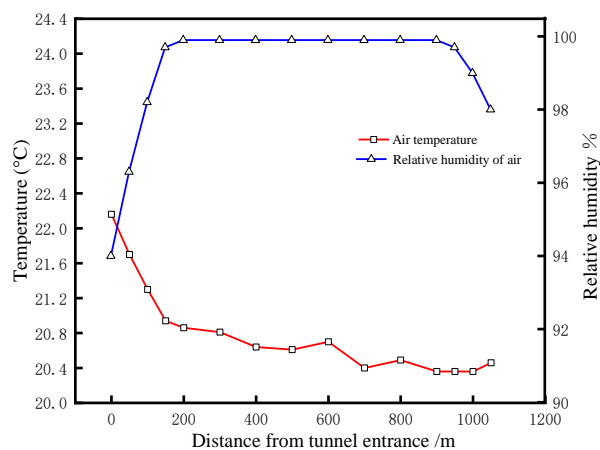
traffic tunnels. In general, the temperature drop curve of the tunnel wall is similar to that of the air.
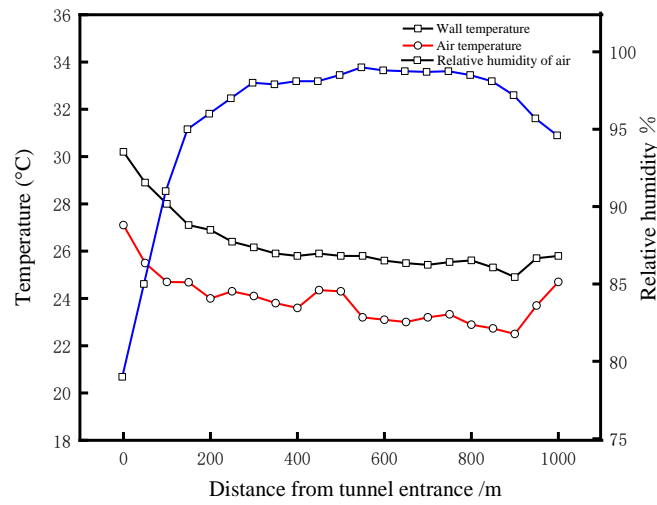
(**a**)
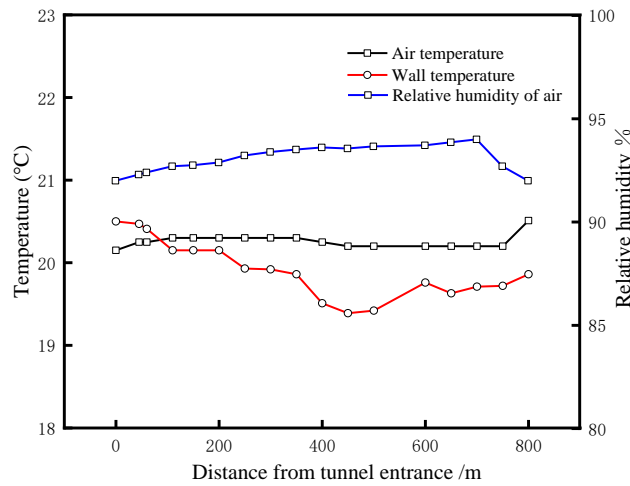
(**b**)

(**c**)

Figure 8. Variation curve of air temperature, relative humidity, and wall temperature at each measuring point of traffic tunnel. (**a**) Xianyou Power Station. (**b**) Dagangshan Power Station. (**c**) Jinping I Power Station.

The test day had light rain and thus was affected by the weather. It can be seen from Figure 8b that the air temperature and relative humidity of each measuring point were relatively stable, and the relative humidity of all measuring points was greater than 90%. Only at the end of the traffic tunnel did the air temperature and wall temperature increase slightly due to the influence of the factory building. The average wall temperature at the entrance and end of the traffic tunnel was slightly higher than that at the middle section, and the fluctuation range was not large on the whole.

The field test of the air inlet heat transfer characteristics of the underground traffic corridor of Jinping I Power Station was carried out, and the variation law of air temperature and humidity at the measurement points outside and inside the incoming traffic tunnel with the depth of the traffic tunnel was measured. The measured changes in temperature and humidity at the entrance and exit of the traffic tunnel are shown in Figure 8c. From the air temperature change curve at the entrance and exit of the traffic tunnel of Jinping I Power Station in Figure 8c, it can be seen that in the summer working conditions, with the increase of the depth of the traffic tunnel, the air temperature gradually decreased and finally tended to be stable. It can be seen that the air temperature at the entrance of the traffic tunnel was 22.1 °C, and after cooling by the traffic tunnel, the temperature stabilized at 20.4 °C, decreasing by 1.7 °C. On the contrary, the relative humidity of the air gradually increased from 94% and finally stabilized at 100%.

4.5. Comparative Analysis and Verification of Heat and Moisture Transfer Effect in Underground Corridor

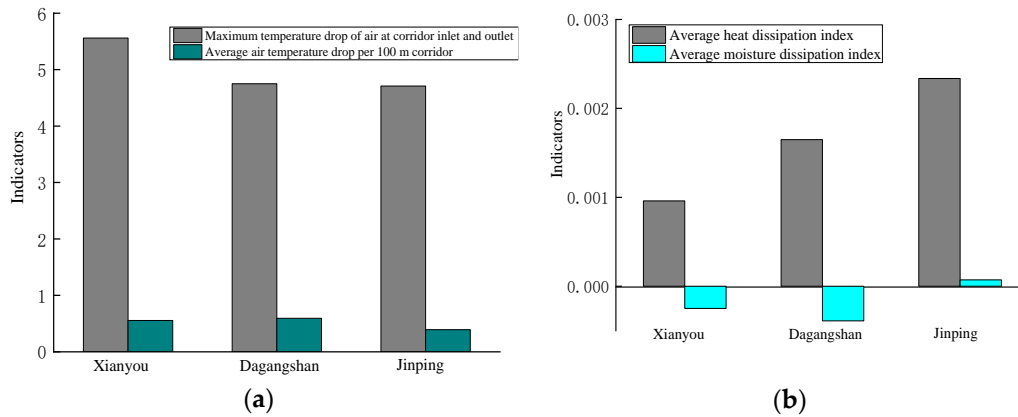4.5.1. Comparison of Heat and Moisture Transfer Indexes

In this paper, the ventilation heat dissipation and moisture dissipation of the underground corridors are obtained through the field measurement of the Xianyou Power Station, Dagangshan Power Station, and Jinping I Power Station. At the same time, the maximum temperature dropper unit length and the average heat dissipation and moisture dissipation indices of the underground traffic tunnels of each power station are obtained in summer, as shown in Table 2. The comparison of various indexes for the power plant is shown in Figure 9.

Table 2. Average moisture dissipation index of the underground traffic tunnel test of each power station.

Name of Power Station	Season	Air Volume (kg/s)	Maximum Temperature Drop (°C)	Maximum Temperature Dropper 100 m Length (°C/HM)	Heat Dissipation Index δ (kW/m^2·s)	Heat Dissipation Index Delta (g/m^2·s)
Xianyou Power Station	Summer	4.6	5.56	0.55600	0.00096	−0.00025
Dagangshan Power Station	Summer	46.38	4.75	0.59375	0.00165	−0.00039
Jinping I Power Station	Summer	100.63	4.71	0.39250	0.00234	0.00007

By comparing and analyzing the ventilation and heat transfer characteristics of the underground corridors of various hydroelectric plants in summer conditions, the underground corridors have a cooling effect on the air flowing through. It can be seen from Figure 9a that the Xianyou Power Station traffic tunnel has the lowest cooling effect on the air flowing through because, during the test process, the air intake into the Xianyou Power Station traffic tunnel was very small, only 4.6 kg/s. At the same time, under summer conditions, the traffic tunnels of Xianyou Power Station and Dagangshan Power Station had negative moisture dissipation into the inflow air, that is, the air was dehumidified. The reasons are analyzed to be as follows: for Dagangshan Power Station, the weather was rainy on the test day, and the humidity of the outdoor air reached 100% saturation For Xianyou Power Station, because Xianyou is located in a subtropical climate zone, the

climate is humid and the relative humidity of the outdoor air is saturated, and thus the traffic tunnel still dehumidifies the air flowing through these two power stations in summer. For Jinping I Power Station, it can be seen that the average moisture dissipation of the traffic tunnel to the air is 0. Figure 9b shows the maximum cooling capacity of each power station traffic tunnel for the air that flows through. It can be seen that there is little difference in the effect of temperature drop after being converted into a corridor with a length of 100 m.


Figure 9. Comparison of underground corridor indexes of power plants in different regions. (**a**) Indicators of heat dissipation and moisture dissipation. (**b**) Temperature drop indicator.

In summary, the authors think that the heat and moisture transfer effect of air flowing through underground corridors is affected by inlet air parameters (velocity, temperature, and humidity), corridor cross-sectional size, corridor wall temperature, traffic tunnel length, and other factors.

4.5.2. Mathematical Model Verification

Based on field-measured data on heat and moisture transfer in underground corridors of the abovementioned power plants, the mathematical models of heat and moisture transfer in underground corridors are compared and verified. The air parameters at the entrance of the underground corridors of each power station, cross-section size, length, and wall temperature of the corridors were obtained by actual measurement, which were brought into the mathematical calculation model of heat and moisture transfer of the corridors, and the theoretical calculation formulas of heat and moisture transfer of each power station along the length direction of the corridors were obtained, respectively. The changes in the measured air temperature and humidity in the field are compared with those of the theoretical calculation formulas, and the comparison results are shown in Figure 10.

Figure 10 shows that the measured field value in the underground corridors of each power station is consistent with the theoretical formula in the trend of the temperature and moisture content on the whole. When the dimensionless distance L is from 0.15 to 0.7, the relative error between the theoretical and measured values of the temperature and moisture content is 8% and 0.8%, respectively. When the dimensionless distance is outside the range, the relative error is large, especially when the dimensionless distance is equal to 0.85, and the relative errors of temperature and moisture content reach the maximum of 40% and 30%, respectively. This is because the air temperature and humidity at the entrance of the corridor are greatly affected by the outdoor environment, and the air parameters at the end of the corridor are greatly affected by the operating equipment in the plant.

(**a**)

(**b**)
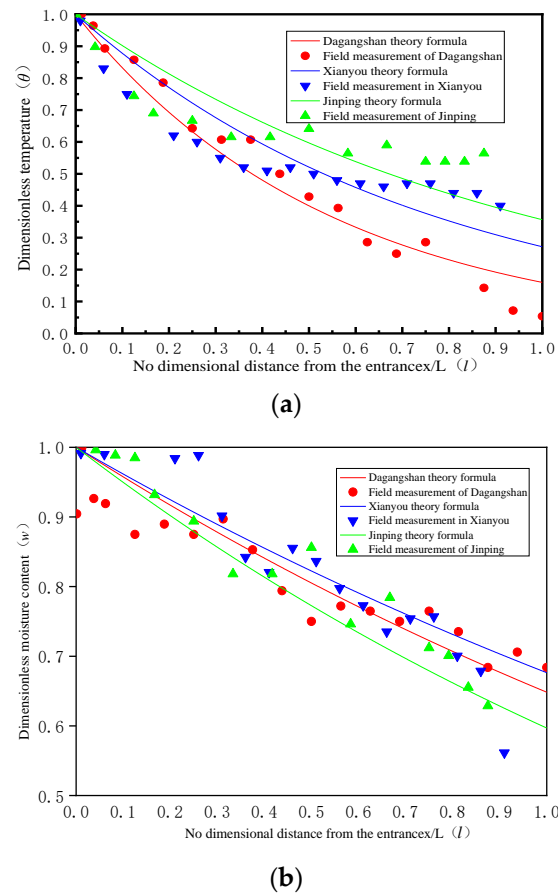
Figure 10. Comparison of the measured and theoretical calculation model of each power station. (**a**) Temperature. (**b**) Moisture content.

5. Analysis of Heat and Humidity Transfer in Circular and Rectangular Corridors

*5.1. The Influence of Each Factor on the Tunnel*

Applying the corridor formula above, the variation law of air temperature and humidity in ventilation corridors with different shapes and structures is studied below. Figure 11 is a schematic diagram of heat and moisture transfer in circular and rectangular corridors. In the circular tunnel along the axis, a small distance dx is taken, and the heat balance equation is established there.

Comparing the simplified circular corridor with the arched and rectangular corridors in practical engineering, it is found that the temperature and humidity of the air flowing through the corridor gradually approach the relatively stable rock mass temperature in the flow process. The rate of change of airflow temperature along its path has the following form.

$$\frac{t_x - t_n}{t_0 - t_n} = e^{-kx}$$

where k is a function of air volume, wall heat transfer capacity, and tunnel surface area. The moisture exchange between the tunnel wall and air depends on the variance of the partial pressure water vapor between them. When the partial pressure of water vapor in the air is greater than the saturated partial pressure of water vapor at the wall temperature, or when the wall temperature is lower than the dew point temperature of the air, the air is dried (wall condensate). On the contrary, when the moisture content of the wall exceeds the equilibrium humidity of the wall material corresponding to the relative humidity of the air, it humidifies the airflow (wall moisture dissipation), and the greater the difference, the

greater the wall moisture dissipation. Of course, in the process of dispersing moisture, if the wall cannot get a timely water supplement, it will gradually transform into a relatively dry state.

(a)

(b)
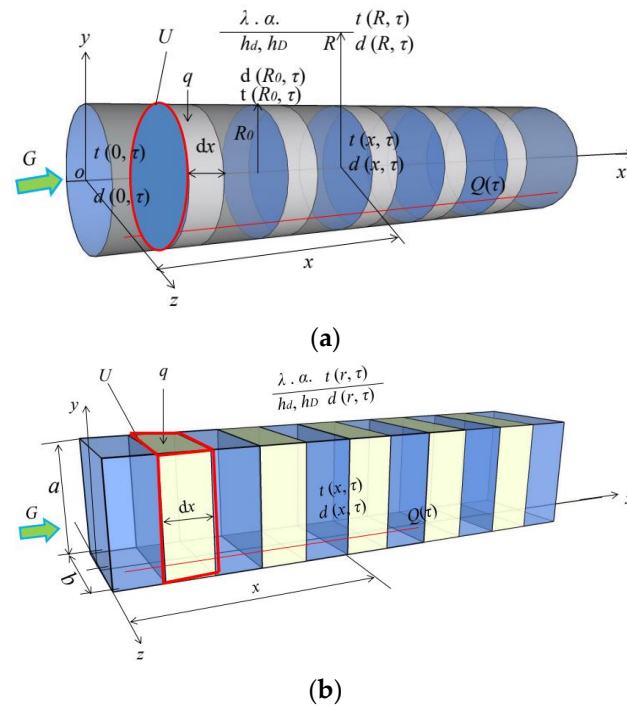
Figure 11. Schematic diagram of the micro-element segmentation of circular corridor and rectangular corridor. (**a**) Circular corridor. (**b**) Rectangular corridor.

In order to more clearly reflect the relationship between air temperature, humidity, and enthalpy in underground corridors and the factors in the calculation formula of the above theoretical model, firstly, it must be known that the arch tunnel of Xianyou Power Station is equivalent to a circular corridor of equivalent diameter. Then, the boundary condition parameters of Xianyou Power Station (Table 3) are applied to the simplified circular corridor model, arched corridor, and rectangular corridor with equivalent diameter. The curves of dimensionless temperature, moisture content, and enthalpy with various factors are shown in Figures 12–14.

Table 3. Comparison of the measured and theoretical calculation model of each power station (summer).

Project	Parameter	Project	Parameter
Corridor wall temperature t_T	293.65 K	Corridor height H	5.5 m
Outdoor temperature t_0	303.65 K	Arch height h of arched corridor	2 m
Corridor width W	7.5 m	Arch radius r_0 of arched corridor	4.52 m
Velocity of air supply	0.5 m/s	Heat transfer coefficient q	1.5 W/(m^2·°C)
Heat source Q in corridor	0 W	Moisture transfer coefficient h_D	0.00045 kg/(m^2·s)

Figure 12 shows that the curves of air temperature, moisture content, and enthalpy in the corridor decrease with the increase of corridor depth, heat, and moisture transfer coefficient. When the air supply velocity and corridor radius increase, the curves show the opposite trend.
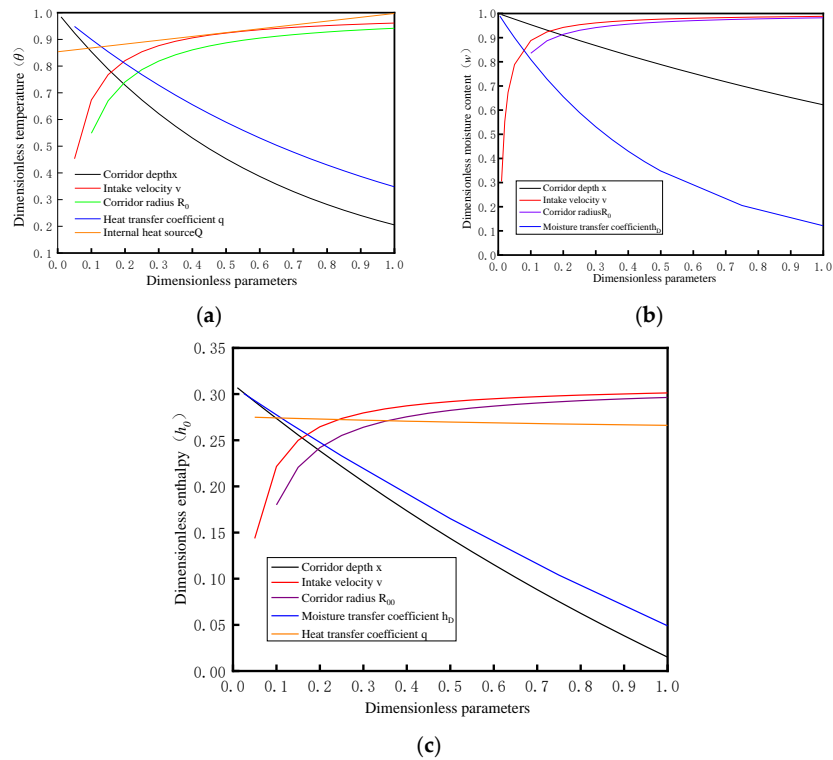
Figure 12. The curve of air parameters with various factors in circular corridor. (**a**) Temperature. (**b**) Moisture content. (**c**) Enthalpy.

Figure 13 shows that the influence of velocity, heat, and moisture transfer coefficient and air inlet velocity on the air parameter curve is consistent with that of the circular corridor. However, the curves of air temperature, moisture content, and enthalpy in the arch corridor increase slowly with the increase of corridor height and width. The vault height and arch radius have little effect on temperature and moisture content.
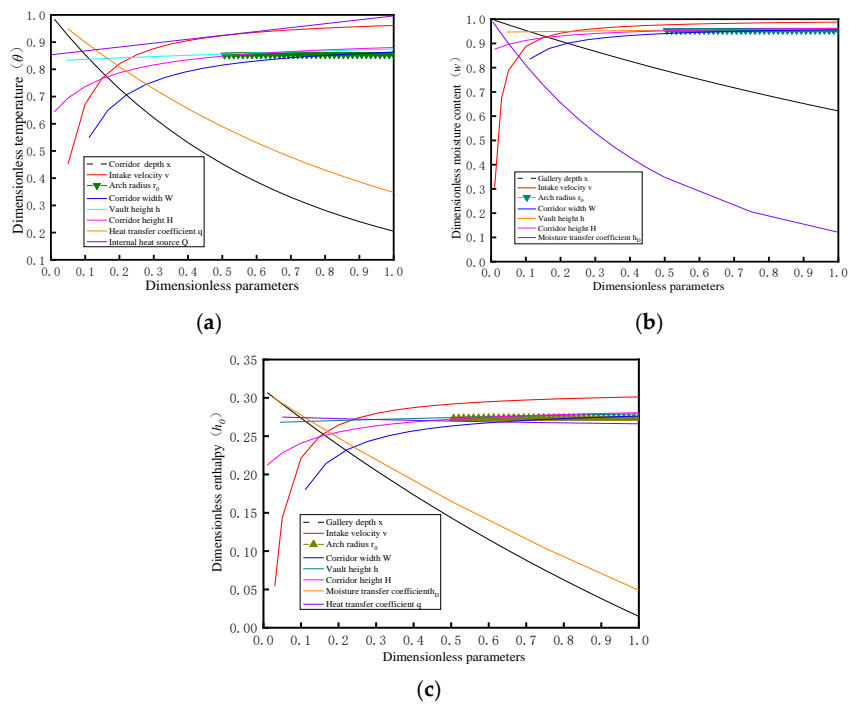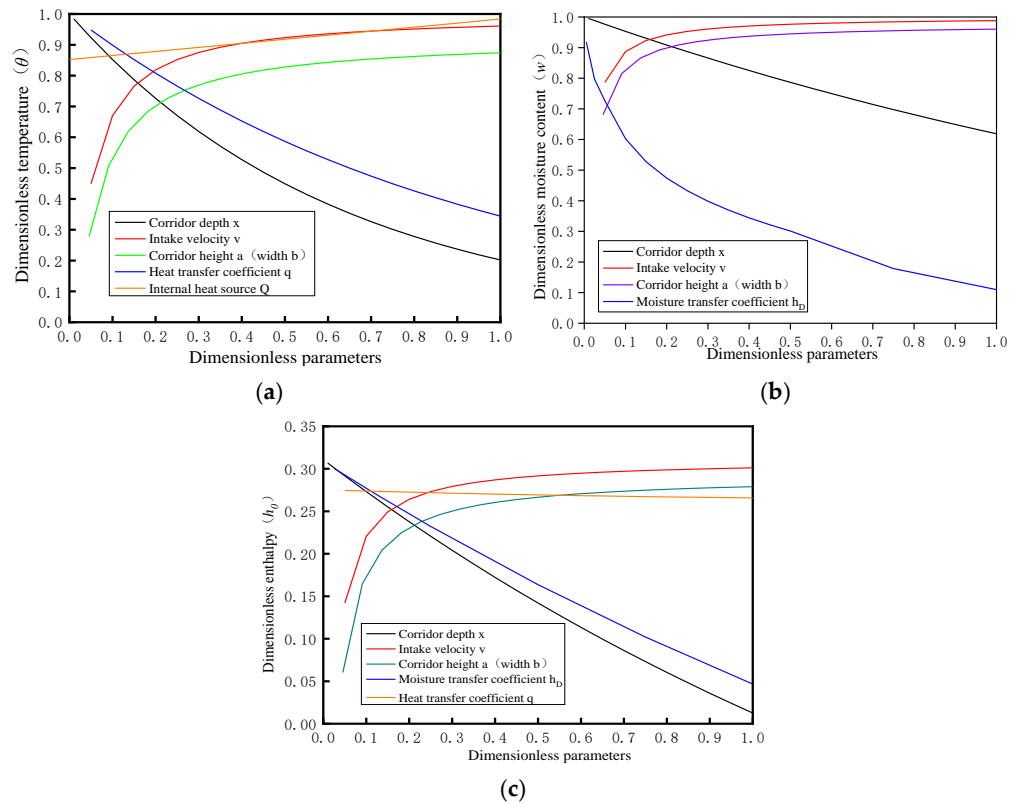

Figure 13. The curve of air parameters with various factors in arch corridor. (**a**) Temperature. (**b**) Moisture content. (**c**) Enthalpy.

Figure 14 also shows that the influence of velocity, heat, and moisture transfer coefficient and air inlet velocity on the air parameter curve is consistent with that of the circular corridor. The curves of air temperature, moisture content, and enthalpy in the rectangular corridor increase significantly with the increase of corridor height or width.

Figure 14. The curve of air parameters with various factors in rectangular corridor. (**a**) Temperature. (**b**) Moisture content. (**c**) Enthalpy.

5.2. Influence of Different Corridor Shapes on Heat and Humidity Transfer

Based on the measured corridor size parameters of Xianyou Power Station, air parameters at 15:00 on August 19 were selected and applied to the model of calculation of the heat and humidity transfer of the arch corridor. At the same time, the mathematical models of the heat and moisture transfer of the circular, arched, and rectangular underground corridors are compared under three working conditions: equal cross-sectional area, equal equivalent diameter, and equal cross-sectional perimeter (Table 4), and the distribution of the air temperature and moisture content along the length of the underground corridors is compared. Field test values are compared with theoretical calculation results, as shown in Figures 15–17.

Table 4. Contrast between field measurement and theoretical model.

Content	Shape	Cross-Sectional Area (m²)	Equivalent Diameter (m)	Cross-Sectional Perimeter (m)	Calculation Formula of Temperature and Moisture Content
Measured	Arch	52.5	7.47	28.1	
Theory	Arch	52.5	7.47	28.1	$t_x = 18 + 11.92e^{-8.03\times10^{-4}x}$ $d_x = 0.01188 - 5.9\times10^{-4}\times e^{-1.2\times10^{-4}x}$
	Circular	52.5	8.18	25.68	$t_x = 18 + 11.92e^{-7.34\times10^{-4}x}$ $d_x = 0.01188 - 5.9\times10^{-4}\times e^{-1.1\times10^{-4}x}$
	Rectangle	52.5	7.25	29	$t_x = 18 + 11.92e^{-8.29\times10^{-4}x}$ $d_x = 0.01188 - 5.9\times10^{-4}\times e^{-1.24\times10^{-4}x}$

Table 4. *Cont.*

| Content	Shape	Cross-Sectional Area (m^2)	Equivalent Diameter (m)	Cross-Sectional Perimeter (m)	Calculation Formula of Temperature and Moisture Content
	Arch	52.5	7.47	28.1	$t_x = 18 + 11.92e^{-8.03 \times 10^{-4}x}$
	Circular	43.8	7.47	23.46	
	Rectangle	55.8	7.47	29.88	$d_x = 0.01188 - 5.9 \times 10^{-4} \times e^{-1.2 \times 10^{-4}x}$
	Arch	52.5	7.47	28.1	$t_x = 18 + 11.92e^{-8.03 \times 10^{-4}x}$ $d_x = 0.01188 - 5.9 \times 10^{-4} \times e^{-1.2 \times 10^{-4}x}$
	Circular	62.88	8.95	28.1	$t_x = 18 + 11.92e^{-6.7 \times 10^{-4}x}$ $d_x = 0.01188 - 5.9 \times 10^{-4} \times e^{-1.01 \times 10^{-4}x}$
	Rectangle	49.35	7.03	28.1	$t_x = 18 + 11.92e^{-8.54 \times 10^{-4}x}$ $d_x = 0.01188 - 5.9 \times 10^{-4} \times e^{-1.28 \times 10^{-4}x}$
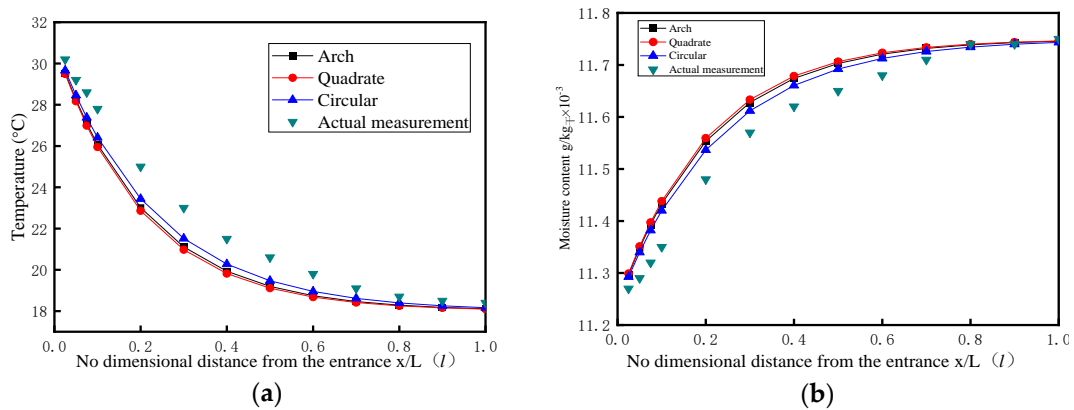
Figure 15. Comparison of measured and calculated values of air parameters of the underground corridor (equal cross-sectional area). (**a**) Temperature. (**b**) Moisture content.
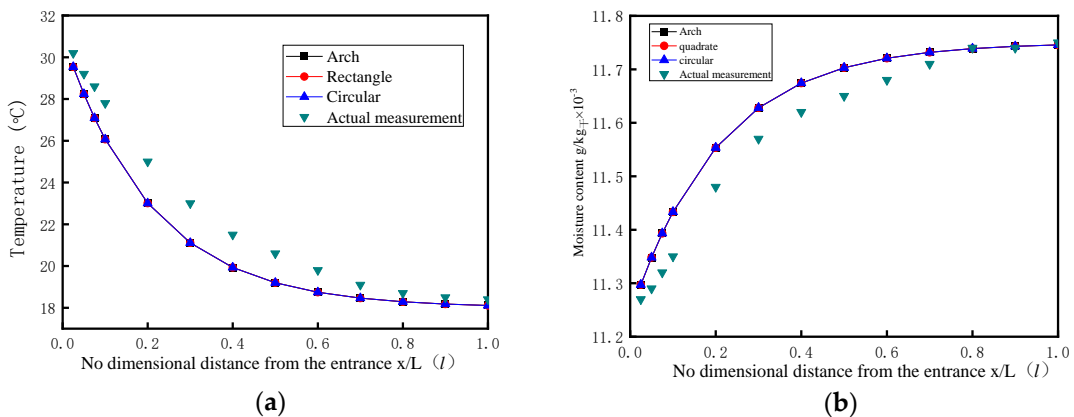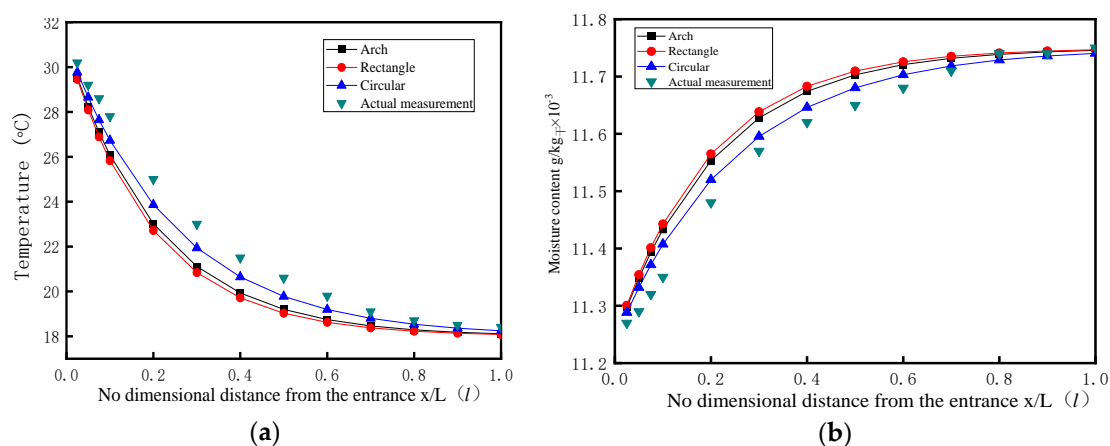

Figure 16. Comparison of measured and calculated values of air parameters of the underground corridor (equivalent diameter). (**a**) Temperature. (**b**) Moisture content.

Figures 15–17 show that with the increase of air depth along the corridor, the temperature gradually cools and the moisture content gradually increases. At the same time, the transfer of heat and moisture from the corridor wall to the air is closely related to the shape and size of the structure cavern. Under the same cross-sectional area, the larger the cross-sectional perimeter of the three underground corridors, the better the heat and moisture transfer effect of the corridor under the same conditions. Under the same cross-sectional perimeter, the smaller the cross-sectional area, the better the heat and moisture transfer effect of the corridor under the same conditions. It can be seen from the above figure that the heat and moisture transfer effect between the inner wall of the rectangular corridor and the air is the best, followed by the arched corridor and circular corridor. The results show

that under the same cross-sectional area, the average temperature drop and humidity of the rectangular corridor are 0.25% and 0.3% higher than that of the arch corridor, and 0.8% and 0.9 higher than that of the circular corridor. Under the condition of constant section circumference, the average temperature drop and humidity of the rectangular corridor are 0.51% and 0.62% higher than that of the arch corridor and 1.37% and 1.58 higher than that of the circular corridor. When the equivalent diameter is the same, there is almost no difference in the heat and humidity transfer effect of the three shaped corridors. Comparing the temperature and humidity difference between the theoretical model and the measured value, the error between the measured value and the theoretical model of the rectangular corridor is the largest, whether it is an equal cross-sectional area, equivalent diameter, or equal cross-sectional perimeter. After calculation, under the condition of an equal cross-section perimeter, the measured temperature is related to the theoretical calculation of the rectangular corridor. The maximum error of value is 9.39%, and the maximum error of moisture content is 0.82%. In the case of equivalent diameter, the maximum error between the measured temperature and the theoretical calculation value of the rectangular corridor is 8.22%, and the maximum error of moisture content is 0.74%. Under the condition of an equal cross-sectional area, the maximum error between the measured temperature and the theoretical calculation value of a rectangular corridor is 8.82%, and the maximum error of the moisture content is 0.78%. The reasons for the errors are analyzed as follows: In the process of solving the theoretical calculation model, the wall temperature is simplified as an isothermal surface, but in the actual underground corridor, there is a slight temperature difference between the wall temperature at the entrance and exit of the corridor. By comparing the measured data with the theoretical calculation model of temperature and humidity distribution in the corridor, it can be seen that the corridor heat and humidity model can better describe the variation law of indoor air parameters in underground caverns, and it has high accuracy and reliability and so can be applied to the prediction and analysis of practical projects.

Figure 17. Comparison between measured and calculated values of air parameters of the underground corridor (equal cross-section circumference). (**a**) Temperature. (**b**) Moisture content.

6. Conclusions

In this study, the effect of heat and humidity transfer for deeply buried underground corridors is studied through theoretical and field tests. Relevant factors are considered in the analysis of changes in temperature, moisture content, and enthalpy. The comparison shows that the theoretical solution and the field test results are in good agreement. The main conclusions are as follows:

(1) By solving the differential equation according to the initial conditions and boundary conditions, the mathematical analytic formula of the air temperature distribution in the corridor of a rotating surface of infinite length can be obtained.

The mathematical analytic formula of air relative humidity and temperature distribution along the corridor is $t_{x,\tau} = t_0 + \left(\frac{Q}{qU} - t_0 + t_T\right)\left(1 - e^{-\frac{qUx}{cG}}\right)$

$$\varphi(x, \tau) = \frac{B}{p_{q, b}(x, \tau)} \cdot \frac{d_D + (d_0 - d_D)e^{-\frac{h_D Ux}{G}}}{0.622 + d_D + (d_0 - d_D)e^{-\frac{h_D Ux}{G}}} \times 100\%$$

(2) The effect of heat and humidity transfer in underground corridors was tested on-site through three hydropower stations. The maximum dispersion coefficient among the hydropower stations is 0.00234 (kW/m²·s), observed at the Jinping Power Station. The minimum is 0.00096 (kW/m²·s) for Xianyou Power Station. The maximum temperature drop index of Xianyou Power Station is the largest, which is 5.56 °C.

(3) The heat and humidity transfer effect between a corridor and the air is related to the size and shape of the corridor. With the same cross-sectional area, the larger the perimeter of the corridor, the better the heat and humidity transfer effect between the corridor and the air. The smaller the cross-sectional area with the same perimeter, the better the heat and moisture transfer effect between the corridor and the air. Under the same cross-sectional area, the average temperature drop and humidity of a rectangular corridor are 0.25% and 0.3% higher than that of an arch corridor and 0.8% and 0.9% higher than that of a circular corridor. Under the condition of constant section circumference, the average temperature drop and humidity of a rectangular corridor are 0.51% and 0.62% higher than that of an arch corridor and 1.37% and 1.58% higher than that of a circular corridor. When the equivalent diameter is the same, there is almost no difference in the heat and humidity transfer effect of the three shaped corridors. Rectangular corridors may have better ventilation effects in practical projects.

We have observed that the direction and efficiency of heat and humidity transfer in tunnels may vary under different seasons. This phenomenon presents a promising avenue for future research, necessitating further in-depth investigation. Additionally, we will give serious consideration to the impact of seasonal changes on heat and humidity transfer within corridors in our forthcoming work.

Nomenclature

CFD	Computational Fluid Dynamics
DEA	Data Envelopment Analysis
$t(x, \tau)$	τ Air temperature at the depth x m of the corridor at all times, °C
$t(f(x, y'), \tau)$	τ Temperature of the rock wall of the corridor time, °C
t_0	Air temperature at the entrance of the corridor
$f(x, y')$	Equivalent radius of the rotating surface corridor, m
U	Wet circumference of the cross-section of the rotating curved corridor, m
x	Distance within the corridor from the entrance of the corridor, m;
v	Air flow rate, m/s
B	Local atmospheric pressure
d	Moisture content, g/kg
G	Air flow, kg/s
Re	Reynolds criterion
h_D	Mass diffusion flux per unit surface area per unit time
h_d	Mass transfer coefficient driven by air moisture difference, kg/(m²·s)
Q	Heat source intensity, W/m
τ	Time, s
d_0	Moisture content of air at the entrance of corridor, g/kg
d_D	Moisture content of rock mass wall, g/kg
λ	Wall thermal conductivity, W/(m · °C)
α	Surface heat transfer coefficient, W/(m²·°C)
C	Equivalent diameter of underground corridor, m
H	Height of arched corridor, m
φ	Relative humidity of the air, %
$P_{q,b}$	The partial pressure of the air, Pa
W	Width of arched corridor, m
n	The angle of the vault arch of the arched corridor, (°)
r_0	Radius of arch corridor vault arc, m
θ	Dimensionless temperature
l	Dimensionless distance
h_0	Dimensionless enthalpy
w	Dimensionless moisture content

References

1. Wang, S.H. Present Situation and Prospect of Hydropower Development in China. *Henan Water Conserv. South—North Water Divers.* **2021**, *50*, 26–27.
2. Zhang, Z.Q.; Wang, S.; Pan, M.Z.; Lv, J.S.; Lu, K.; Ye, Y.S.; Tan, D.L. Utilization of hydrogen-diesel blends for the improvements of a dual-fuel engine based on the improved Taguchi methodology. *Energy* **2024**, *292*, 130474. [CrossRef]
3. Hu, X.Y.; Wang, T.; Chen, K.; Ye, P.Q.; Zhang, L.G. Research on control system for improving the grid-connected efficiency of small hydropower. *Energy Rep.* **2023**, *9*, 772–783. [CrossRef]
4. Dai, L.T.; Gao, J.; Huang, S.D.; Tang, X.L. Variable-speed constant-frequency hydropower generation technology and its development. *Autom. Electr. Power Syst.* **2020**, *44*, 169–177.
5. Guo, J.N.; Li, A.G.; Ma, Y.Q.; Che, J.G.; Li, J.X.; Niu, S.F.; Deng, L.H.; Wang, D.; Che, L.F. A theoretical and applied convective heat transfer model for deep-buried underground tunnels with non-constant wall temperature. *Energy Build.* **2023**, *294*, 113210. [CrossRef]
6. Dang, Y.R. Experimental Study on Heat Absorption and Release Characteristics of Rough Air Intake Gallery in Hydropower Engineering. Master's Thesis, Xi'an University of Architecture and Technology, Xi'an, China, 2012.
7. Ma, M.R.; Chen, J.; Xiao, Y.M.; Gao, X.K.; Liu, Y.; Yuan, X.Q. Field tests and analyses of thermal and humidity environment and heating and cooling capacity of air intake tunnels into underground plants. *Energy Rep.* **2022**, *8* (Suppl. S10), 665–672. [CrossRef]
8. Fadnes, S.F.; Assadi, M. Utilizing Wastewater Tunnels as Thermal Reservoirs for Heat Pumps in Smart Cities. *Energies* **2024**, *17*, 4832. [CrossRef]

9. Liu, C.; Cheng, H.H.; Nie, W.J.; Jiang, S.L.; Chen, L.F.; Lin, P.; Zhong, M.H. Study on smoke propagation in tunnel construction of a hydropower station: A full-scale fire experiment. *J. Saf. Sci. Resil.* **2023**, *4*, 188–202. [CrossRef]

10. Guo, J.N.; Li, A.G.; Zhang, C.; Li, J.X.; Che, J.G.; Xiong, J.; Jiao, X.Q. Modeling effective heat transfer and ventilation in deeply buried underground tunnels. *Int. J. Therm. Sci.* **2023**, *184*, 107949. [CrossRef]

11. Zhang, Z. Theoretical analysis on heat transfer through wall in underground big-space building under ventilated condition. *J. Water Resour. Water Eng.* **2009**, *20*, 48–51.

12. Zhao, H.Z. Calculation of cold air cooling in tunnel. *HVAC* **1975**, *1*, 42–46.

13. Jiang, Y. Basic Research on Thermal Physics of Natural Environment Temperature Difference Utilization in Underground Space. Ph.D. Thesis, Tsinghua University: Beijing, China, 1985.

14. Pan, Y.; Li, Y.; Shen, X. Research on the air temperature and humidity transfer law in the ventilation corridor of the underground powerhouse of pumped storage power station in summer. *Refrigeration* **2017**, *43*, 39–42, 47. [CrossRef]

15. Yoo, J.-O.; Kim, J.-S. A numerical study of the effects of the ventilation velocity on the thermal characteristics in underground utility tunnel. *J. Korean Tunn. Undergr. Space Assoc.* **2017**, *19*, 29–39. [CrossRef]

16. Kang, F.; Li, Y.; Tang, C. Numerical study on airflow temperature field in a high-temperature tunnel with insulation layer. *Appl. Therm. Eng.* **2020**, *179*, 115654. [CrossRef]

17. Zeng, Y.H.; Tao, L.L.; Ye, X.Q.; Zhou, X.H.; Fang, Y.; Fan, L.; Liu, X.R.; Yang, Z.X. Temperature reduction for extra-long railway tunnel with high geotemperature by longitudinal ventilation. *Tunn. Undergr. Space Technol.* **2020**, *99*, 103381. [CrossRef]

18. Chen, Q.G. Thermophysical theoretical basis of underground cold storage building design. *J. Refrig.* **1980**, *3*, 30–46.

19. Chen, Q.G. Humidity calculation theory in porous envelope structure. *J. Civ. Environ. Eng.* **1984**, *3*, 1–18.

20. Cucumo, M.; Cucumo, S.; Montoro, L.; Vulcano, A. A one-dimensional transient analytical model for earth-to-air heat exchangers, taking into account condensation phenomena and thermal perturbation from the upper free surface as well as around the buried pipes. *Int. J. Heat Mass Transf.* **2008**, *51*, 506–516. [CrossRef]

21. Su, H.; Liu, X.B.; Ji, L.; Mu, J.Y. A numerical model of a deeply buried air-earth-tunnel heat exchanger. *Energy Build.* **2012**, *48*, 233–239. [CrossRef]

22. Liu, J.Y.; Wang, H.X.; Wang, N.; Zhou, L. Evaluation research of the control effectiveness of underground defensive projects thermal and humidity environment. *Appl. Mech. Mater.* **2013**, *273*, 28–33. [CrossRef]

23. Tan, X.; Chen, W.; Yang, D.; Dai, Y.; Wu, G. Study on the influence of airflow on the temperature of the surrounding rock in a cold region tunnel and its application to insulation layer design. *Appl. Therm. Eng.* **2014**, *67*, 320–334. [CrossRef]

24. Wang, Q. The Cooling Effect of Greenhouse Soil Heat Exchange System Research on Influencing Factors. Master's Thesis, Northwest Agriculture and Forestry University, Xianyang, China, 2023. [CrossRef]

25. Zhou, Y.; Zhao, Y.; Zhang, Z.Q.; Pu, S.; Zhang, H. Influence of duct layout parameters of tunnel ventilation on gas migration characteristics. *Sci. Technol. Eng.* **2021**, *21*, 12718–12726.

26. Tang, Z.Q.; Gao, K.; Tao, C.F.; Liu, Y.J.; Qi, Z.P. The influence of tunnel aspect ratio on the gas temperature distribution in advancing tunnel. *Tunn. Undergr. Space Technol.* **2024**, *149*, 105818. [CrossRef]

27. Shao, Z.Y.; Li, Y.; Cui, H.H.; Yu, B.S.; Cong, H.Y. Numerical investigation of longitudinal location and heat release rate of fire source on neutral plane height and induced flow in longitudinal sloping tunnel fires under natural ventilation. *Int. J. Therm. Sci.* **2024**, *200*, 108981. [CrossRef]

28. Jędrzejuk, H.; Orzełowska, F. Analysis of the Operation of Smoke Exhaust Ventilation in the Metro's Technological Corridor Based on Numerical Simulation of Selected Locations of Fire. *Energies* **2023**, *16*, 849. [CrossRef]

29. Liu, X.C. Formation Mechanism of Thermal and Humid Environment and Energy-Saving Control Strategy of Underground Hydropower Station. Ph.D. Thesis, Chongqing University, Chongqing, China, 2014.

30. Wang, T.; Ma, M.R.; Ren, Z.L.; Yuan, X.Q.; Gao, X.K.; Xiao, Y.M. Numerical analysis of heat and mass transfer in separated ventilation of deeply buried long air intake tunnels. *Energy* **2024**, *304*, 132091. [CrossRef]

31. Jia, C.J.; Xie, Y.H.; Dai, L.; Shi, C.H.; Lei, M.F.; Zheng, Y.N. Detailed thermal environment classification of high geothermal tunnel based on thermal comfort indices. *Build. Environ.* **2024**, *266*, 112135. [CrossRef]

32. Chen, S.S.; Geng, S.B.; Li, Y.; Xiao, M.X. Application of GAHP in energy-saving evaluation index system for ventilation and air-conditioning systems in protective engineering. *Prot. Eng.* **2013**, *35*, 73–78.

33. Eckert, E.R.; Drake, R.M. *Analysis of Heat and Mass Transfer*; Hang, Q., Ed.; Science Press: Beijing, China, 1983; Volume 845.

34. Deshmukh, M.K.; Sodha, M.S.; Sawhney, R.L. Effect of depth of sinking on thermal performance of partially underground building. *Int. J. Energy Res.* **1951**, *15*, 391–403. [CrossRef]

35. Wang, X.J.; Zhang, S.Y.; Peng, D.M.; Wang, J. Application of porous media drying mechanism in thermal dehydration of lignite. *Coal Convers.* **2011**, *34*, 82–86.

36. Mao, J.F.; Han, X. *Theory and Application of Heat and Humidity in Underground Engineering*; China Architecture and Architecture Press: Beijing, China, 2009.

37. Wang, X.L. *Experimental Study of Cooling Effect in Underground Tunnel of Hydropower Station*; Xi'an University of Architecture and Technology: Xi'an, China, 2008.

38. Kuzenov, V.V.; Ryzhkov, S.V.; Varaksin, A.Y. Development of a Method for Solving Elliptic Differential Equations Based on a Nonlinear Compact-Polynomial Scheme. *J. Comput. Appl. Math.* **2024**, *451*, 116098. [CrossRef]